UC Berkeley

UC Berkeley Previously Published Works

Title

Finite element models predict the location of microdamage in cancellous bone following uniaxial loading

Permalink

https://escholarship.org/uc/item/1qc668jb

Journal

Journal of Biomechanics, 48(15)

ISSN

0021-9290

Authors

Goff, MG
Lambers, FM
Sorna, RM
et al.

Publication Date

2015-11-01

DOI

10.1016/j.jbiomech.2015.10.023

Peer reviewed

eScholarship.org Powered by the California Digital Library
University of California

Author Manuscript

Author Manuscript

Author Manuscript

Author Manuscript

HHS Public Access

Author manuscript

J Biomech. Author manuscript; available in PMC 2016 November 26.

Published in final edited form as:

J Biomech. 2015 November 26; 48(15): 4142–4148. doi:10.1016/j.jbiomech.2015.10.023.

Finite Element Models Predict the Location of Microdamage in Cancellous Bone Following Uniaxial Loading

M.G. Goff[1,2], **F.M. Lambers**[2], **R.M. Sorna**[2], **T.M. Keaveny**[3], and **C.J. Hernandez**[1,2,4]

[1]Department of Biomedical Engineering, Cornell University, Ithaca, NY, USA

[2]Sibley School of Mechanical and Aerospace Engineering, Cornell University, Ithaca, NY, USA

[3]Department of Mechanical Engineering, University of California, Berkeley, CA, USA

[4]Hospital for Special Surgery, New York City, NY, USA

Abstract

High-resolution finite element models derived from micro-computed tomography images are often used to study the effects of trabecular microarchitecture and loading mode on tissue stress, but the degree to which existing finite element methods correctly predict the location of tissue failure is not well characterized. In the current study, we determined the relationship between the location of highly strained tissue, as determined from high-resolution finite element models, and the location of tissue microdamage, as determined from three-dimensional fluoroscopy imaging, which was performed after the microdamage was generated in-vitro by mechanical testing. Fourteen specimens of human vertebral cancellous bone were assessed (8 male donors, 2 female donors, 47–78 years of age). Regions of stained microdamage, were 50–75% more likely to form in highly strained tissue (principal strains exceeding 0.4%) than elsewhere, and generally the locations of the regions of microdamage were significantly correlated ($p < 0.05$) with the locations of highly strained tissue. This spatial correlation was stronger for the largest regions of microdamage (≥ 1,000,000 μm^3 in volume); 87% of large regions of microdamage were located near highly strained tissue. Together, these findings demonstrate that there is a strong correlation between regions of microdamage and regions of high strain in human cancellous bone, particularly for the biomechanically more important large instances of microdamage.

Keywords

bone mechanics; finite element model; microdamage

Corresponding Address: Christopher J. Hernandez, Ph.D., 219 Upson Hall, Cornell University, Ithaca, NY 14853, Phone: (607) 255-5129, Fax: (607) 255-1222, cjh275@cornell.edu.

CONFLICT OF INTEREST STATEMENT

The authors declare no potential conflict of interest.

Publisher's Disclaimer: This is a PDF file of an unedited manuscript that has been accepted for publication. As a service to our customers we are providing this early version of the manuscript. The manuscript will undergo copyediting, typesetting, and review of the resulting proof before it is published in its final citable form. Please note that during the production process errors may be discovered which could affect the content, and all legal disclaimers that apply to the journal pertain.

Author Manuscript Author Manuscript Author Manuscript Author Manuscript

1.0 INTRODUCTION

Impaired bone tissue material toughness has been associated with increased risk of fragility fracture in patients with diabetes and patients undergoing bisphosphonate treatment (de Waard et al., 2014; Shane et al., 2014). Recent efforts to understand failure mechanisms in bone have concentrated on tissue material toughness and resistance to the formation of tissue microdamage. Small amounts of microdamage (occupying less than 2% of the tissue) result in large reductions in stiffness, strength, and fatigue life of cancellous bone (Hernandez et al., 2014; Lambers et al., 2013), highlighting the potential importance of tissue microdamage to clinical fractures.

High resolution finite element models, derived from three-dimensional images of trabecular bone microstructure, are the primary means of estimating tissue level stress and strain in cancellous bone. Modern high-resolution finite element models of cancellous bone are capable of predicting apparent yield strength and are often used to estimate the amount of tissue damage generated by overloads (Baumann et al., 2015; Bayraktar et al., 2004; Morgan et al., 2004; Nawathe et al., 2013; Niebur et al., 2001). However, there have been few attempts to relate finite element-derived tissue strains to microdamage measured using histology. The few studies that have addressed the topic have not done so directly, either demonstrating that the total volume of microdamage generated is correlated with the volume of failed tissue predicted by finite element models (Shi et al., 2010; Yeni et al., 2003) or that the locations of “severe” microdamage display greater than average local tissue stresses (Nagaraja et al., 2005; Nagaraja et al., 2011). None of the studies reported to date have asked how well finite element models predict the locations of microdamage generation within cancellous bone. Finite element models of cancellous bone suggest that loading mode (apparent tension, compression, shear) influences tissue level yielding (Bayraktar and Keaveny, 2004; Morgan et al., 2004). Experimental investigations have shown that loading mode influences the amount and location of microdamage (Wang et al., 2005; Wu et al., 2013), specifically tensile loading causes greater amounts of tissue microdamage than compressive loading (Lambers et al., 2014). Hence, the relationship between finite element derived tissue strains and microdamage generation is likely influenced by apparent loading mode.

The long-term goal of the current work is to understand how tissue level toughness in cancellous bone influences whole bone fracture. Here, we determine how well finite element models are able to predict the locations of microdamage generation in cancellous bone. Specifically we determine the spatial relationship between microdamage and tissue level strain predicted by finite element models following two different loading modes: apparent tension and apparent compression.

2.0 METHODS

Here we perform an additional analysis of specimens described in a previous study (Lambers et al., 2014). In section 2.1 we review the experimental methods of our prior study and in sections 2.2–2.5 we describe the methods novel to the current study.

Author Manuscript Author Manuscript Author Manuscript Author Manuscript

2.1 Study design

Specimens were collected from the L4 vertebral bodies of 10 donors (n=14, 8 male, 2 female, 47–78 years of age, tissue from NDRI, Philadelphia, PA). The donors had no history of metabolic bone disease and displayed no obvious vertebral deformities. Cylinders of cancellous bone, 8 mm diameter and nominally 25–30 mm height, oriented in the cranial-caudal direction were collected. Specimens were stored at −20 °C. Prior to loading, micro-computed tomography images of each sample were obtained at an isotropic voxel size of 10 μm (Scanco μCT 20, Scanco Medical AG, Brüttisellen, Switzerland). Additionally, specimens were stained with xylenol orange (0.5 mM in PBS, 2 h) prior to loading to label preexisting damage.

Specimens were potted into brass fixtures using bone cement (as previously described (Bevill et al., 2009)) and subjected to 0.8% strain (apparent yield) in tension (n=6) or compression (n=8) at a rate of 0.5%/s. Apparent level yield strain and Young's Modulus were determined from the stress-strain curve. Following loading, the central 5 mm length of each specimen was cut from the center of the exposed gage length with a low speed diamond saw and the specimens were submitted to calcein staining (0.5 mM in PBS, 2h) to identify microdamage generated during loading. Specimens were then embedded undecalcified in methyl-methacrylate. Three-dimensional images of bone and fluorescent labels of microdamage were acquired at a voxel size of $0.7 \times 0.7 \times 5\ \mu m^3$ using serial milling (Slyfield et al., 2009; Slyfield et al., 2012). Bone and fluorescent labels were segmented using manually determined global thresholds. Images were then smoothed to correct for cutting marks left by the serial milling technique. The region of interest examined included the central region of the specimen image (5.4 mm diameter, 4 mm height) thereby avoiding microdamage caused during specimen preparation. To eliminate the possibility of non-specific surface staining (thin layers of stain that occur on bone surfaces that are ignored when making manual microdamage counts), microdamage stain within 5.6 μm of the surface of the trabeculae was removed from the images. Microdamage generated by loading was identified as bone tissue displaying calcein (post-loading stain) in the absence of xylenol orange (pre-loading stain).

2.2 Finite element modeling

To reduce computational expense, micro-computed tomography were down-sampled to an isotropic voxel size of 20 μm using a region averaging technique (Bevill et al., 2009). A voxel size of 20 μm is less than one-fourth the mean trabecular thickness and is sufficient for high resolution finite element models of bone (Guldberg et al., 1998; Niebur et al., 1999). Bone was identified using a global threshold determined from the Otsu method (Otsu, 1979). Each voxel was converted into a linear elastic, eight node brick element. Linear elastic models indicated the locations of the greatest stresses/strains, where the majority of microdamage sites should initiate. Elements were assigned a Young's modulus of 10 GPa and a Poisson's ratio of 0.3 (Bevill et al., 2009). The caudal surface of the model was fully constrained and a 0.8% apparent strain was applied to the cranial surface to simulate the physical loading conditions (either tensile or compression). Finite element models were implemented using Olympus (Adams et al., 2004) on a Sun Constellation Linux Cluster (Ranger; TACC, TX, USA). Tissue principal strains were measured at the centroid of every

Author Manuscript Author Manuscript Author Manuscript Author Manuscript

element (Niebur et al., 2001). The most positive principal strains are referred to as tissue tensile principal strains and the most negative principal strains are referred to as tissue compressive principal strains.

2.3 Probability of microdamage at finite element modeled strain

To determine how well local tissue strains predict the locations of microdamage, the probability of observing microdamage was determined as a function of principal strain magnitude. Images of microdamage were down-sampled from to match the image resolution used in the finite element models (20 μm). To prevent noise from altering measures of microdamage, regions of microdamage within 28 μm of each other were considered to be part of the same microdamage site and microdamage sites smaller than 64,000 μm^3 (eight voxels) were characterized as noise and removed from the images (as we have done previously (Lambers et al., 2014)). Images of microdamage were then registered to the finite element models accounting for rotation, translation, scaling and shearing (Amira version 5.4 Visage Imaging, San Diego, CA, USA). Tissue principal strains were binned (0.04% bin size) and the probability of observing microdamage at was estimated as follows:

$$Probability = \frac{DV_{at\ strain}}{BV_{at\ strain}} \quad \text{Eq. 1}$$

where $DV_{at\ strain}$ is the damage volume and $BV_{at\ strain}$ is the bone volume at the given strain magnitude.

2.4 Spatial correlation of microdamage and highly strained tissue

The spatial correlation between microdamage and highly strained tissue was assessed in two ways: 1) a spatial correlation based on volume (volume-based method) and 2) a spatial correlation of discrete objects (object number-based method) (Figure 1) (Goff et al., 2014). The volume-based method determined the degree to which microdamage volume was more likely to be near highly strained tissue than other regions of the bone. The volume-based spatial correlation was expressed as the ratio of the amount of microdamage volume near highly strained tissue to that of an equal amount of bone volume (selected at random) that was near highly strained tissue. A ratio of 1.0 indicated no spatial correlation, a ratio greater than 1.0 indicated a positive spatial correlation (microdamage was more likely to be near highly strained tissue than other bone volume), and a value less than 1.0 indicated negative spatial correlation (microdamage was less likely to be near highly strained tissue than other bone volume). The volume-based spatial correlation was then repeated to ask the converse question: if highly strained tissue was more likely to be near microdamage than other regions of the bone. The object number-based spatial correlation was expressed as the percentage of microdamage sites near highly strained tissue as well as the converse question (the percentage of highly strained tissue sites near microdamage). For both spatial correlation methods, proximity was determined at distances ranging from 0 μm to 60 μm (~ half of the average trabecular thickness).

The spatial relationship between microdamage and large tissue level strains will vary based on the magnitude of tissue strains characterized as “large.” A parametric analysis was performed to determine the tissue strain magnitude that best predicted the locations of

Author Manuscript Author Manuscript Author Manuscript Author Manuscript

microdamage. Highly strained tissue was defined as tissue experiencing principal strains that exceeded a value ranging from 0.1% to 1%. As with the images of microdamage, regions of highly strained tissue smaller than 64,000 μm^3 (eight voxels) were characterized as noise and not included in the spatial correlation analysis.

2.5 Statistical analyses

The magnitudes of principal strain in regions of microdamage and the rest of the bone were compared using a two-tailed paired t-test. Regression analysis was used to determine the relationship between strain predicted by finite element modeling and the probability of microdamage. The spatial correlations determined using the volume-based method were tested for a difference from 1.0 using a two-tailed paired t-test, (a value of 1.0 indicated no spatial correlation). All data is presented as mean ± SD. Statistical tests were conducted using JMP Pro (v.11, 2013, SAS Institute Inc., Cary, NC, USA).

3.0 RESULTS

The relationship between microdamage and local tissue strain differed between specimens loaded in tension and those loaded in compression. In specimens submitted to loading under apparent tension, the local principal strains were greater at microdamage than away from microdamage (tension: 0.32 ± 0.09% v. 0.20 ± 0.05%, compression: 0.14 ± 0.03% v. 0.11 ± 0.02%, Figure 2A). Additionally, the probability of observing microdamage at a location in the microstructure was positively correlated with local tensile principal strain but was not predictive ($p<0.0001$, $R^2=0.30$, Figure 3A). Local compressive principal strain showed no correlation with microdamage. Overall, the probability of observing microdamage was 50–75% greater at tissue tensile strains above 0.4% as compared to the average incidence of microdamage (Figure 3A).

In specimens submitted to apparent compression, the tissue principal strains were greater at microdamage than away from microdamage (tension: 0.14 ± 0.02% v. 0.12 ± 0.01%, compression: 0.31 ± 0.06% v. 0.22 ± 0.03%, Figure 2B). The probability of observing microdamage at a location in the microstructure was positively correlated with local compressive principal strains but was not predictive ($p<0.0001$, $R^2=0.08$, Figure 3B). No correlation between the probability of microdamage and tissue tensile principal strain was observed. Overall, the probability of microdamage was 50–75% greater at tissue tensile strains above 0.4% as compared to the average incidence of microdamage (Figure 3B).

Microdamage was located near highly strained tissue. The volume-based spatial correlation indicated a significant positive correlation between highly strained tissue and microdamage volume (Figure 4 and Supplementary Materials Figure S1,S2). Over half of microdamage sites were located at tissue experiencing a principal strain of 0.4% or higher; however, less than half of the highly strained tissue sites were located at microdamage (Figure 5 and Supplementary Materials Figure S3).

The magnitude of strain used to classify highly strained tissue had limited influence on the volume-based spatial correlations. The volume-based spatial correlations were greatest when the magnitude of strain used to define highly strained tissue was 0.4% or greater (Figure 4B

Author Manuscript Author Manuscript Author Manuscript Author Manuscript

and Supplementary Materials Figure S2). The object number-based spatial correlation, however, was quite sensitive to the strain magnitude used to classify highly strained tissue (Figure 5C,D and Supplementary Materials Figure S3).

As large microdamage sites (sites over 1,000,000 μm^3 in volume) have been shown to be the most influential biomechanically (Goff et al., 2015), we also examined the spatial correlation assays looking only at large microdamage and highly strained tissue sites. Most of the microdamage volume (86% ± 8%) was located in a small number of large microdamage sites (microdamage sites exceeding 1,000,000 μm^3 in volume). Similarly, most of the highly strained tissue volume (89% ± 5%) was located in a few large sites. When only large microdamage and highly strained tissue sites were considered, strong volume based and object number-based spatial correlations were observed between microdamage sites and highly strained tissue sites (Figure 6A,B and Supplementary Materials Figure S4,S5).

4.0 DISCUSSION

Here we present the first three dimensional examination of the spatial correlation between microdamage and local tissue strains in human cancellous bone. We found that microdamage was most likely to occur at the greatest tissue level principal strains. The largest microdamage sites were spatially correlated with the largest regions of high tissue strain determined with finite element models. Therefore our findings demonstrate surprising effectiveness of linear elastic finite element models to predict the locations of the largest (and most biomechanically relevant (Goff et al., 2015)) microdamage sites.

While the linear elastic finite element models were useful for predicting the locations of the largest microdamage sites, the models were not able to predict the location of all of the microdamage sites. Since the strains predicted by linear elastic finite element models will deviate from the actual tissue strain once the tissue begins to yield, we did not expect the tissue strains to dictate the location of all of the microdamage but we did expect most of the sites experiencing the greatest tissue strains to coincide with microdamage. Regions with the greatest tissue strain magnitudes were more likely to develop microdamage, but even at the locations of greatest tissue strain, the probability of observing microdamage was relatively low (~20%, Figure 3). Furthermore, if we consider only the locations with the greatest tissue strains (right hand side of Figure 5B) we see that locations of the greatest tissue strains were rarely near microdamage.

There are a number of strengths to the current study that support our conclusions. First, the spatial correlation between highly strained tissue and microdamage was determined using three different assays (probability of microdamage at strain magnitudes, volume-based spatial correlation and object number-based spatial correlation). Second, both the analysis of microdamage and tissue level strain was performed in three dimensions. Three dimensional analysis reduces the variability in the microdamage measurement by using the entire specimen (Ehlert et al., 2011) and is able to take into consideration out-of-plane spatial relationships between microdamage and tissue level strain.

Author Manuscript Author Manuscript Author Manuscript Author Manuscript

There are some limitations that must be considered in interpreting our results. First, as mentioned in our interpretation above, the current analysis used linear elastic finite element models, which do not account for the effects of tissue yielding on the stress/strain distribution within cancellous bone. However, the current study examined loading to apparent yield and at such small magnitudes of apparent strain there are only negligible differences between linear and non-linear models in terms of the amounts of tissue exceeding yield (Niebur et al., 2001). Second, microdamage was stained using a bulk fluorochrome stain, which stains most but not all regions of permanent deformation in bone tissue (Sun et al., 2010). Hence, the relationship seen between local tissue stress/strain and microdamage should be considered a conservative estimate.

Our findings provide insight into the best approaches for improving models of microdamage formation in cancellous bone. The most common advancement in high resolution finite element modeling is the use of a nonlinear constitutive model, which has been shown to enable prediction of apparent yield properties (Bayraktar and Keaveny, 2004; Morgan et al., 2004) and describe changes in stress/strain distribution after tissue level yield occurs. However, initial tissue yielding in nonlinear models will coincide with regions of the greatest tissue strains observed in linear elastic models. Our observation that few of the microdamage sites were near the locations of greatest tissue strain in the linear elastic finite element models suggests that constitutive models with tissue nonlinearities alone would provide relatively little improvement toward predicting the locations of tissue microdamage. A more likely explanation for microdamage not being located at the predicted locations of greatest tissue strain is heterogeneity in tissue material properties. When a heterogeneous tissue modulus is included in linear finite element models, the distribution of stress/strain is altered (Mulder et al., 2007; Renders et al., 2011). Therefore, incorporating tissue heterogeneity is more likely to improve the prediction of the locations of microdamage than including tissue nonlinearities.

Our findings are consistent with prior reports showing that regions of microdamage experience greater tissue strains (Nagaraja et al., 2005; Nagaraja et al., 2011). The magnitude of tissue compressive principal strain at microdamage and away from microdamage in the current study (0.32%, 0.20%) was similar to the results reported by Narajaga and colleagues (2011) (0.33%, 0.19%). Additionally, in the current work, microdamage was spatially correlated with tissue experiencing a tissue principal strain greater than 0.4%, a tissue strain similar to the tensile yield strain criterion used in prior work (0.33% –0.61%) (Bayraktar et al., 2004; Morgan et al., 2004; Nawathe et al., 2013). However, in prior work the compressive yield strain criterion was larger than the tensile yield strain criterion while in the current work the same strain magnitude was associated with microdamage in tension and compression. A likely explanation for the difference between our findings and others is that prior studies were estimating the tissue level yielding, which is not the same as microdamage generation.

In conclusion, we have demonstrated that linear elastic finite element models can be used to predict the locations where large microdamage sites will form in cancellous bone following either tensile or compressive loading. Furthermore, incorporating heterogeneity in tissue level material properties or a stochastic model of damage generation are more likely to

Author Manuscript Author Manuscript Author Manuscript Author Manuscript

improve the predictive capabilities of finite element models than including nonlinearities in the model.

Supplementary Material

Refer to Web version on PubMed Central for supplementary material.

Acknowledgments

Research reported in this publication was supported by the National Institute of Arthritis and Musculoskeletal and Skin Diseases of the National Institutes of Health (U.S) under Award Number AR057362 (PI CJH). The content is solely the responsibility of the authors and does not necessarily represent the official views of the National Institutes of Health. We acknowledge use of human vertebral bodies provided by the National Disease Research Interchange (NDRI), with support from NIH grant 8U42OD011158-22. We thank Ivana H. Yi and Michael G. Jekir for performing the mechanical tests.

References

Adams, MF.; Bayraktar, HH.; Keaveny, TM.; Papadopoulos, P. Year Ultrascalable Implicit Finite Element Analyses in Solid Mechanics with over a Half a Billion Degrees of Freedom. Proceedings of the 2004 ACM/IEEE Conference;

Baumann AP, Shi X, Roeder RK, Niebur GL. The sensitivity of nonlinear computational models of trabecular bone to tissue level constitutive model. Computer methods in biomechanics and biomedical engineering. 2015; 11:1–9. [PubMed: 25959510]

Bayraktar HH, Keaveny TM. Mechanisms of uniformity of yield strains for trabecular bone. Journal of biomechanics. 2004; 37:1671–1678. [PubMed: 15388309]

Bayraktar HH, Morgan EF, Niebur GL, Morris GE, Wong EK, Keaveny TM. Comparison of the elastic and yield properties of human femoral trabecular and cortical bone tissue. Journal of biomechanics. 2004; 37:27–35. [PubMed: 14672565]

Bevill G, Eswaran SK, Farahmand F, Keaveny TM. The influence of boundary conditions and loading mode on high-resolution finite element-computed trabecular tissue properties. Bone. 2009; 44:573–578. [PubMed: 19110082]

de Waard EA, van Geel TA, Savelberg HH, Koster A, Geusens PP, van den Bergh JP. Increased fracture risk in patients with type 2 diabetes mellitus: An overview of the underlying mechanisms and the usefulness of imaging modalities and fracture risk assessment tools. Maturitas. 2014; 79:265–274. [PubMed: 25192916]

Ehlert, K.; O'Brien, R.; Hernandez, C. Statistical power in measures of microscopic tissue damage in cancellous bone. American Society for Bone and Mineral Research; San Diego, CA, USA: 2011. p. MO0052

Goff MG, Chang KL, Litts EN, Hernandez CJ. The effects of misalignment during in vivo loading of bone: Techniques to detect the proximity of objects in three-dimensional models. Journal of biomechanics. 2014; 47:3156–3161. [PubMed: 25001204]

Goff MG, Lambers FM, Nguyen TM, Sung J, Rimnac CM, Hernandez CJ. Fatigue-induced microdamage in cancellous bone occurs distant from resorption cavities and trabecular surfaces. Bone. 2015; 79:8–14. [PubMed: 26008609]

Guldberg RE, Hollister SJ, Charras GT. The accuracy of digital image-based finite element models. Journal of biomechanical engineering. 1998; 120:289–295. [PubMed: 10412392]

Hernandez CJ, Lambers FM, Widjaja J, Chapa C, Rimnac CM. Quantitative relationships between microdamage and cancellous bone strength and stiffness. Bone. 2014; 66:205–213. [PubMed: 24928495]

Lambers FM, Bouman AR, Rimnac CM, Hernandez CJ. Microdamage caused by fatigue loading in human cancellous bone: relationship to reductions in bone biomechanical performance. PLoS One. 2013; 8:e83662. [PubMed: 24386247]

Author Manuscript Author Manuscript Author Manuscript Author Manuscript

Lambers FM, Bouman AR, Tkachenko EV, Keaveny TM, Hernandez CJ. The Effects of tensile-compressive loading mode and microarchitecture on microdamage in Human vertebral cancellous bone. Journal of biomechanics. 2014; 47:3605–3612. [PubMed: 25458150]

Morgan EF, Bayraktar HH, Yeh OC, Majumdar S, Burghardt A, Keaveny TM. Contribution of inter-site variations in architecture to trabecular bone apparent yield strains. Journal of biomechanics. 2004; 37:1413–1420. [PubMed: 15275849]

Mulder L, Koolstra JH, den Toonder JM, van Eijden TM. Intratrabecular distribution of tissue stiffness and mineralization in developing trabecular bone. Bone. 2007; 41:256–265. [PubMed: 17567548]

Nagaraja S, Couse TL, Guldberg RE. Trabecular bone microdamage and microstructural stresses under uniaxial compression. Journal of biomechanics. 2005; 38:707–716. [PubMed: 15713291]

Nagaraja S, Skrinjar O, Guldberg RE. Spatial correlations of trabecular bone microdamage with local stresses and strains using rigid image registration. Journal of biomechanical engineering. 2011; 133:064502. [PubMed: 21744931]

Nawathe S, Juillard F, Keaveny TM. Theoretical bounds for the influence of tissue-level ductility on the apparent-level strength of human trabecular bone. Journal of biomechanics. 2013; 46:1293–1299. [PubMed: 23497799]

Niebur GL, Yuen JC, Burghardt AJ, Keaveny TM. Sensitivity of damage predictions to tissue level yield properties and apparent loading conditions. Journal of biomechanics. 2001; 34:699–706. [PubMed: 11311712]

Niebur GL, Yuen JC, Hsia AC, Keaveny TM. Convergence behavior of high-resolution finite element models of trabecular bone. Journal of biomechanical engineering. 1999; 121:629–635. [PubMed: 10633264]

Otsu N. Threshold Selection Method from Gray-Level Histograms. IEEE Transactions on Systems Man and Cybernetics. 1979; 9:62–66.

Renders GA, Mulder L, van Ruijven LJ, Langenbach GE, van Eijden TM. Mineral heterogeneity affects predictions of intratrabecular stress and strain. Journal of biomechanics. 2011; 44:402–407. [PubMed: 21040918]

Shane E, Burr D, Abrahamsen B, Adler RA, Brown TD, Cheung AM, Cosman F, Curtis JR, Dell R, Dempster DW, Ebeling PR, Einhorn TA, Genant HK, Geusens P, Klaushofer K, Lane JM, McKiernan F, McKinney R, Ng A, Nieves J, O'Keefe R, Papapoulos S, Howe TS, van der Meulen MC, Weinstein RS, Whyte MP. Atypical subtrochanteric and diaphyseal femoral fractures: second report of a task force of the American Society for Bone and Mineral Research. Journal of bone and mineral research. 2014; 29:1–23. [PubMed: 23712442]

Shi X, Liu XS, Wang X, Guo XE, Niebur GL. Effects of trabecular type and orientation on microdamage susceptibility in trabecular bone. Bone. 2010; 46:1260–1266. [PubMed: 20149908]

Slyfield CR Jr, Niemeyer KE, Tkachenko EV, Tomlinson RE, Steyer GG, Patthanacharoenphon CG, Kazakia GJ, Wilson DL, Hernandez CJ. Three-dimensional surface texture visualization of bone tissue through epifluorescence-based serial block face imaging. Journal of microscopy. 2009; 236:52–59. [PubMed: 19772536]

Slyfield CR, Tkachenko EV, Wilson DL, Hernandez CJ. Three-dimensional dynamic bone histomorphometry. Journal of bone and mineral research. 2012; 27:486–495. [PubMed: 22028195]

Sun X, Hoon Jeon J, Blendell J, Akkus O. Visualization of a phantom post-yield deformation process in cortical bone. Journal of biomechanics. 2010; 43:1989–1996. [PubMed: 20382387]

Wang X, Guyette J, Liu X, Roeder RK, Niebur GL. Axial-shear interaction effects on microdamage in bovine tibial trabecular bone. European journal of morphology. 2005; 42:61–70. [PubMed: 16123025]

Wu Z, Laneve AJ, Niebur GL. In vivo microdamage is an indicator of susceptibility to initiation and propagation of microdamage in human femoral trabecular bone. Bone. 2013; 55:208–215. [PubMed: 23459314]

Yeni YN, Hou FJ, Ciarelli T, Vashishth D, Fyhrie DP. Trabecular shear stresses predict in vivo linear microcrack density but not diffuse damage in human vertebral cancellous bone. Annals of biomedical enginering. 2003; 31:726–732.

Author Manuscript Author Manuscript Author Manuscript Author Manuscript

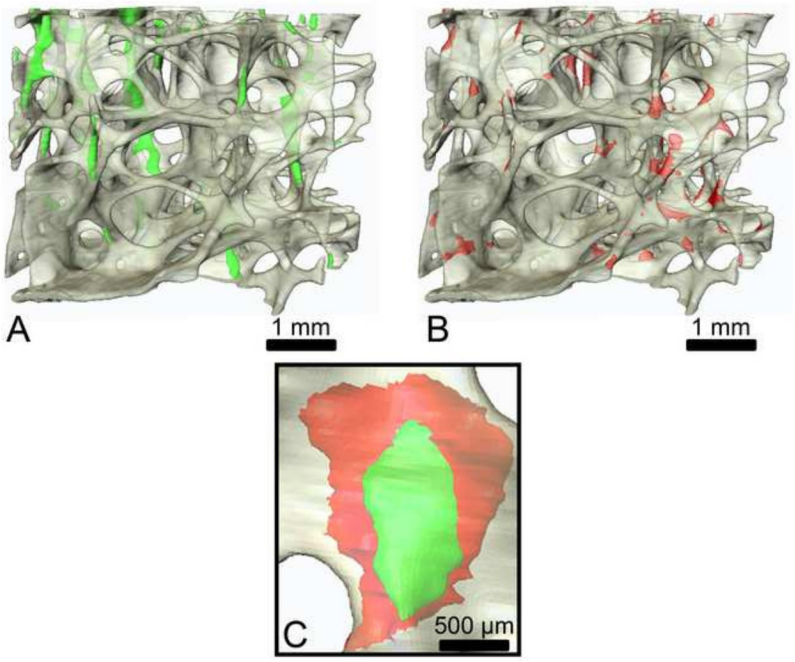

Figure 1.

A specimen of cancellous bone is shown. (A) Highly strained tissue is indicated in green. (B) Microdamage is indicated in red. (C) Image registration was used to determine the spatial associations between microdamage and highly strained tissue.

Author Manuscript Author Manuscript Author Manuscript Author Manuscript

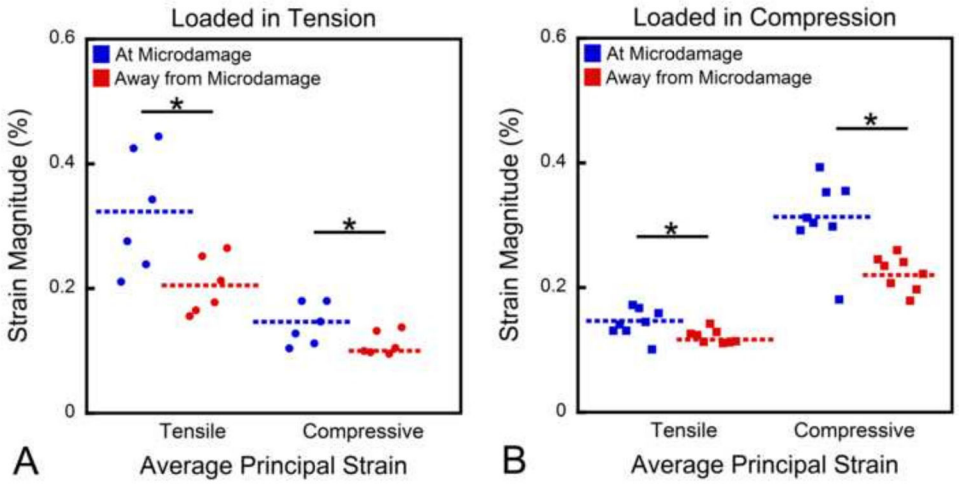

Figure 2.

Tissue tensile and compressive principal strains were greater at locations of microdamage as compared to other regions of the microstructure. ($p<0.05$)

Author Manuscript Author Manuscript Author Manuscript Author Manuscript

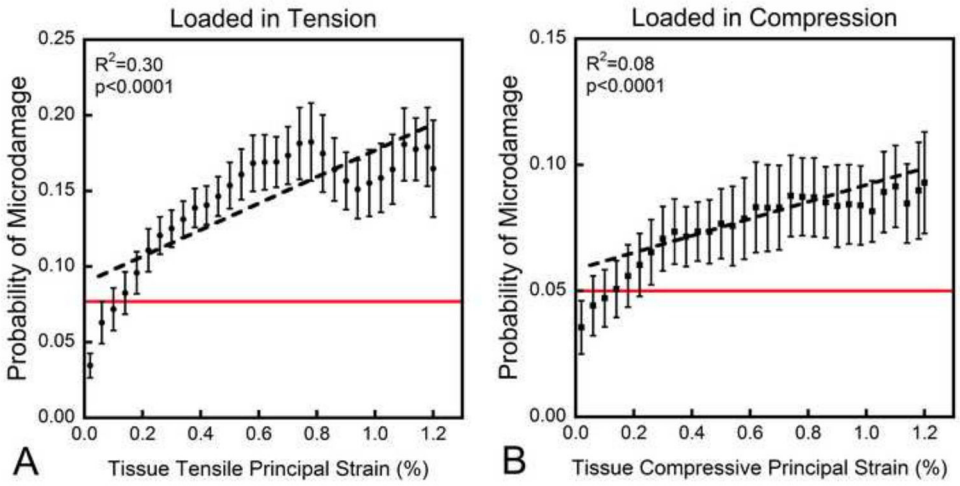

Figure 3.

(A) In specimens loaded in tension, the probability of microdamage was positively correlated with tissue tensile principal strains. (B) In specimens loading in compression, the probability of microdamage was positively correlated with tissue compressive principal strains. The average probability of microdamage occurring in the specimens is shown in red.

Author Manuscript Author Manuscript Author Manuscript Author Manuscript

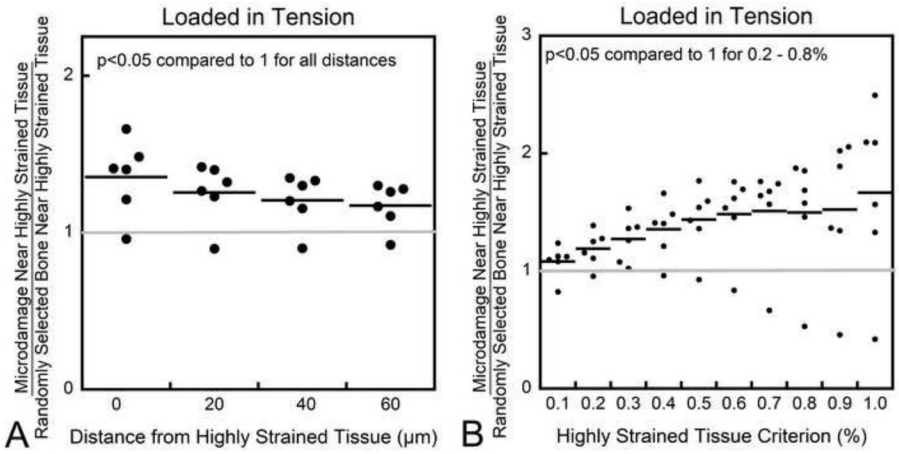

Figure 4.

The volume-based spatial correlations are shown. A value greater than 1.0 indicates a positive spatial correlation. (A) The spatial correlation between microdamage and highly strained tissue (defined as strain greater than 0.4%) with respect to distance between the volumes is shown. (B) The spatial correlation between microdamage and highly strained tissue was greatest when the magnitude of strain used to define highly strained tissue exceeded 0.4%. Similar trends were seen for specimens loaded in compression (see Supplementary Material Figure S1,S2).

Author Manuscript
Author Manuscript
Author Manuscript
Author Manuscript

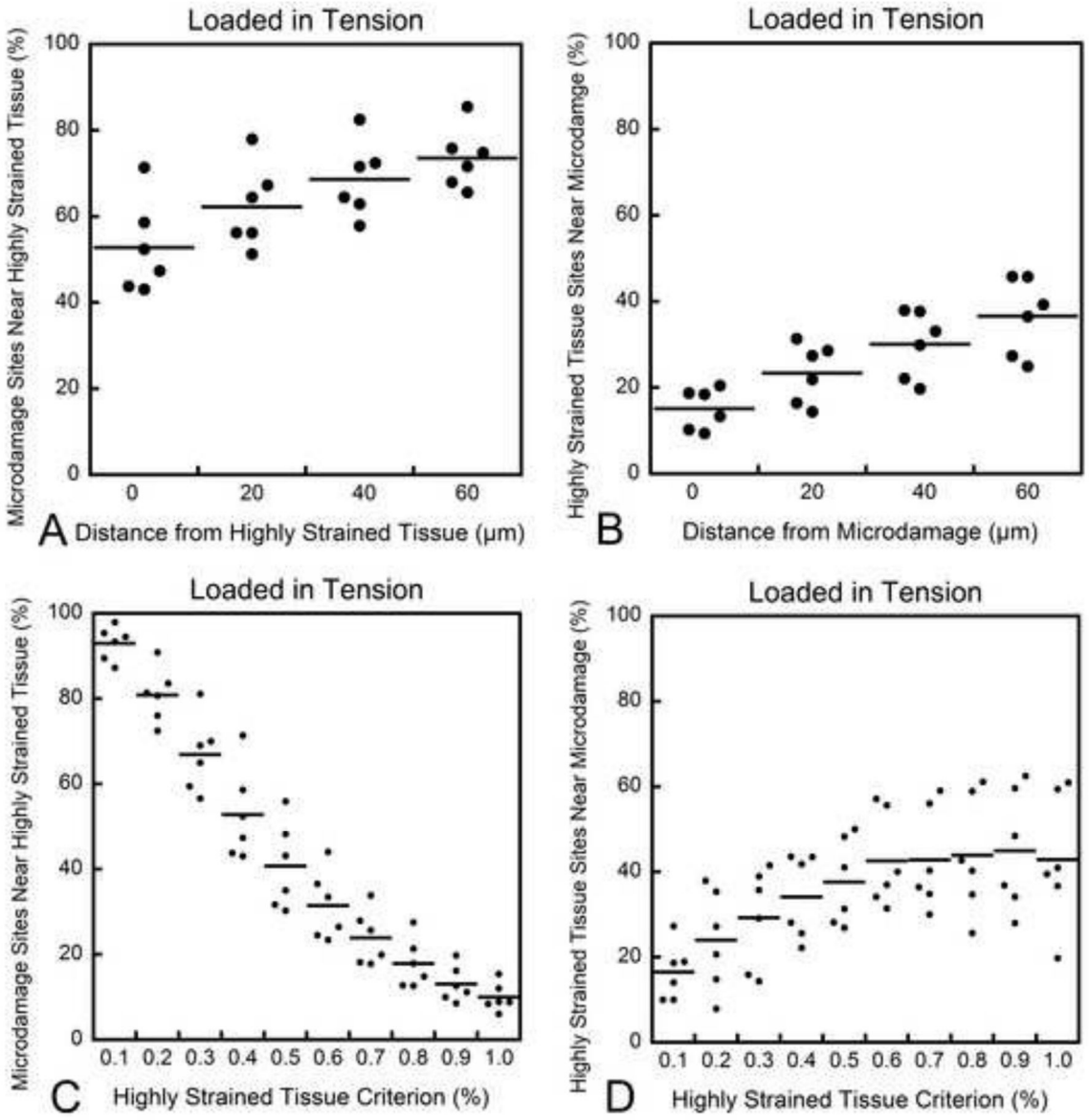

Figure 5.

The object number-based spatial correlations are shown. The percentage of (A) microdamage sites near highly strained tissue and (B) highly strained tissue sites near microdamage increased as the distance between the objects increased. (C) The percentage of microdamage sites near highly strained tissue was inversely proportional to the strain magnitude used to define highly strained tissue. (D) Sites of highly strained tissue were not commonly located near microdamage. Similar trends were seen for specimens loaded in compression (see Supplementary Material Figure S3).

Author Manuscript Author Manuscript Author Manuscript Author Manuscript

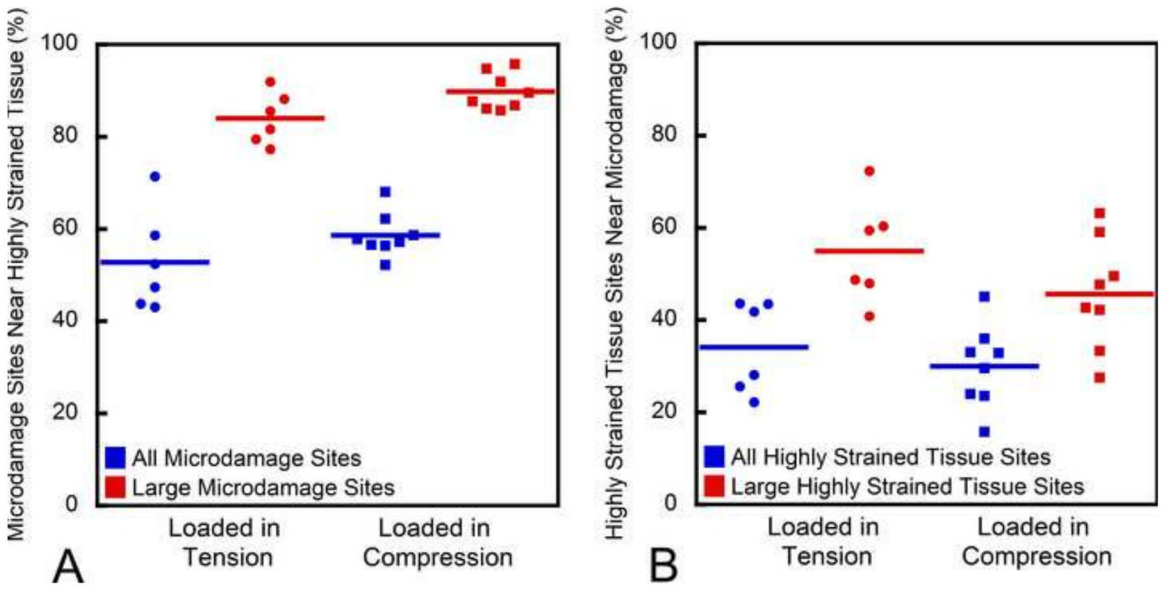

Figure 6.

The object number-based spatial correlation is shown for all microdamage sites as well as only the largest microdamage sites (>1,000,000 μm^3, shown only for coincident locations, distance = 0 μm). When only the largest sites were considered, both the percentage of microdamage sites near highly strained tissue (A) and the percentage of highly strained tissue sites near microdamage (B) increased.